High thermal conductivity and thermal boundary conductance of homoepitaxially grown gallium nitride (GaN) thin films

Yee Rui Koh,[1,*] Md Shafkat Bin Hoque,[1,*] Habib Ahmad,[2,*] David H. Olson,[1,†] Zeyu Liu,[3] Jingjing Shi,[4] Yekan Wang,[5] Kenny Huynh,[5] Eric R. Hoglund,[6] Kiumars Aryana,[1] James M. Howe,[6] Mark S. Goorsky,[5] Samuel Graham,[4,7] Tengfei Luo,[3] Jennifer K. Hite,[8] W. Alan Doolittle,[2,‡] and Patrick E. Hopkins[1,6,9,§]

[1]*Department of Mechanical and Aerospace Engineering, University of Virginia, Charlottesville, Virginia 22904, USA*
[2]*School of Electrical and Computer Engineering, Georgia Institute of Technology, Atlanta, Georgia 30332, USA*
[3]*Department of Aerospace and Mechanical Engineering, University of Notre Dame, Notre Dame, Indiana 46556, USA*
[4]*George W. Woodruff School of Mechanical Engineering, Georgia Institute of Technology, Atlanta, Georgia 30332, USA*
[5]*Department of Materials Science and Engineering, University of California, Los Angeles, California 90095, USA*
[6]*Department of Materials Science and Engineering, University of Virginia, Charlottesville, Virginia 22904, USA*
[7]*School of Materials Science and Engineering, Georgia Institute of Technology, Atlanta, Georgia 30332, USA*
[8]*U.S. Naval Research Laboratory, Washington, D.C. 20375, USA*
[9]*Department of Physics, University of Virginia, Charlottesville, Virginia 22904, USA*

(Received 10 July 2021; accepted 13 September 2021; published 14 October 2021)

Gallium nitride (GaN) has emerged as a quintessential wide band-gap semiconductor for an array of high-power and high-frequency electronic devices. The phonon thermal resistances that arise in GaN thin films can result in detrimental performances in these applications. In this work, we report on the thermal conductivity of submicrometer and micrometer thick homoepitaxial GaN films grown via two different techniques (metal-organic chemical vapor deposition and molecular beam epitaxy) and measured via two different techniques (time domain thermoreflectance and steady-state thermoreflectance). When unintentionally doped, these homoepitaxial GaN films possess higher thermal conductivities than other heteroepitaxially grown GaN films of equivalent thicknesses reported in the literature. When doped, the thermal conductivities of the GaN films decrease substantially due to phonon-dopant scattering, which reveals that the major source of phonon thermal resistance in homoepitaxially grown GaN films can arise from doping. Our temperature-dependent thermal conductivity measurements reveal that below 200 K, scattering with the defects and GaN/GaN interface limits the thermal transport of the unintentionally doped homoepitaxial GaN films. Further, we demonstrate the ability to achieve the highest reported thermal boundary conductance at metal/GaN interfaces through *in situ* deposition of aluminum in ultrahigh vacuum during molecular beam epitaxy growth of the GaN films. Our results inform the development of low thermal resistance GaN films and interfaces by furthering the understanding of phonon scattering processes that impact the thermal transport in homoepitaxially grown GaN.

DOI: 10.1103/PhysRevMaterials.5.104604

I. INTRODUCTION

Gallium nitride (GaN) is a wide band-gap semiconductor suitable for power electronics, high-frequency devices, and light emitting diodes [1,2]. The relatively high phonon thermal conductivity of single-crystal GaN has made it particularly appealing for these aforementioned applications due to its potential to effectively dissipate heat from hot spots and active regions [3–6]. However, this benefit of high phonon thermal conductivity is diminished in most relevant device applications due to phonon scattering from size effects, dopants, isotope disorder, vacancies, and dislocations that result in increased thermal resistances [7–10]. Clearly, the characteristic length scales of GaN films in devices, the required doping for device functionality, and the defects arising from heterogeneous integration of GaN on substrates and submounts can all lead to undesirable phonon scattering and thermal resistances. These, in turn, can lead to device underperformance and failure. Thus, understanding of the dominant phonon scattering processes and origins of reduced thermal conductivities in GaN thin films is of utmost importance to further both material processing and integrated device design initiatives for GaN-based electronics.

There is an extensive list of prior experimental measurements on the thermal conductivity of GaN thin films [11–13]. In general, at room temperature, for GaN films with thicknesses greater than a few micrometers, phonon-boundary scattering and resulting size effects do not play a dominant role in any observed reduction in thermal conductivity. At these length scales, dislocations or grain boundary scattering from heterogeneous growth and isotope or dopant scattering

*These authors contributed equally to this work.
†Present address: Laser Thermal Analysis, Inc., Charlottesville, Virginia 22902, USA.
‡alan.doolittle@ece.gatech.edu
§phopkins@virginia.edu

can be the dominant thermal resistances [6,14,15]. At submicron thicknesses, however, boundary scattering can play a significant role and size effects can reduce the thermal conductivity of GaN films at room temperature [12]. However, isolating the role of size effects on the thermal conductivity of GaN films at these thicknesses can be obfuscated from other defect scattering processes that arise from heterogeneous growth (e.g., dislocations, grain boundaries, etc.) [16]. Similarly, separating the contribution of doping on the thermal conductivity of submicrometer thick GaN films can be challenging due to the difficulty of growing high-quality thin films [12].

In this study, we report on a series of experimental measurements on the cross-plane thermal conductivity of 0.25–2.1 μm thick homoepitaxial GaN films grown on GaN substrates or GaN templated sapphire substrates via metal-organic chemical vapor deposition (MOCVD) and molecular beam epitaxy (MBE). Unlike prior works, we focus on GaN films grown on GaN substrates/templates to better isolate the role of size effects and doping on reductions in the thermal conductivity of GaN thin films. Two different techniques, time domain thermoreflectance (TDTR) [17–21] and steady-state thermoreflectance (SSTR) [22–24], are employed to measure the thermal conductivities. At room temperature, our unintentionally doped (UID) homoepitaxially grown GaN films exhibit some of the highest thermal conductivities reported to date for GaN films of equivalent thicknesses. We attribute this to the lower point-defect concentrations and dislocation density of the homoepitaxially grown films as compared to those of heteroepitaxially grown GaN. As the temperature decreases below 200 K, the dominant source of thermal resistance in the UID films shifts from phonon-phonon scattering to phonon-defect and phonon-boundary scattering. When doped with Mg, the thermal conductivities of the GaN films reduce substantially due to phonon-dopant scattering exhibiting the high influence of doping on GaN thermal resistance. Increasing the dopant concentration from 10^{18} to 10^{19} cm^{-3} decreases the electrical resistance from ~0.85 to 0.30 Ω cm, but results in negligible changes in thermal conductivity. We further demonstrate that high thermal boundary conductance at metal/GaN interfaces can be achieved through *in situ* deposition of aluminum (Al) in ultrahigh vacuum during MBE growth of the homoepitaxial GaN films. Our results indicate that elastic phonon scattering is dominating the thermal transport at this high-quality Al/GaN interface.

II. GROWTH DETAILS OF THE GaN THIN FILMS

Six UID GaN thin films of varying thicknesses (0.25–2.1 μm) are grown on *n*-doped hydride vapor phase epitaxy (HVPE) GaN wafers by MOCVD using a 6 × 2 in. Veeco D-180 reactor refurbished by Agnitron, Inc. We use a V/III ratio of 3000, pressure of 200 Torr, and temperature of 1030 °C with trimethylgallium and ammonia sources for growing these films. Secondary ion mass spectroscopy (SIMS) is used to characterize the impurity concentrations of the films. The silicon (Si), carbon (C), and oxygen (O) impurity concentrations of the GaN films range from 10^{15} to 10^{16} cm^{-3}, as described in detail by Hite *et al.* [25]. The dislocation density of the films is estimated from transmission electron microscopy (TEM) to be on the order of 10^{8} cm^{-2}. All the MOCVD-grown films are cleaned with isopropanol, acetone, methanol, and oxygen plasma [26] prior to *ex situ* Al deposition via electron beam evaporation for TDTR and SSTR transduction [16,27–30].

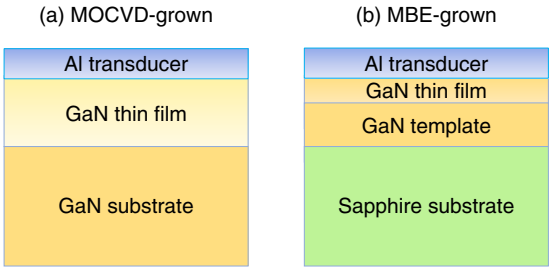

FIG. 1. Schematics of the (a) MOCVD-grown and (b) MBE-grown GaN thin film samples measured in this study.

Six additional samples of 0.4 and 0.8 μm UID and Mg-doped GaN films are grown on HVPE semi-insulating Fe-doped GaN templates on sapphire substrates in a Riber 32 system by metal modulated epitaxy (MME) at the Georgia Institute of Technology. MME is a modified MBE growth technique achieving high crystalline wafer-scale reproducible films by modulating the metal fluxes while keeping the nitrogen flux constant. SIMS characterization at Evans Analytical Group (EAG) reveals the Si, C, and O impurity concentrations of the UID GaN films to be ~1×10^{15}, 1×10^{16}, and 2×10^{17} cm^{-3}, respectively. The Mg-doped GaN films are grown at two different *p*-type conductivity levels of 10^{18} and 10^{19} cm^{-3}. The electrical resistivity of the doped films is characterized by the four-point probe method [31]. The dislocation density of the MBE-grown GaN films is not characterized, however, based on the related literature [32–34], it can be estimated to be in the range of 10^{5}–10^{8} cm^{-2}. Contrary to the MOCVD-grown films, Al is deposited atop the MBE-grown films *in situ* under ultrahigh vacuum. Additional details regarding the cleaning procedure and Al deposition technique of the MBE-grown films are provided in the Supplemental Material [35].

Figure 1 shows the schematics of the GaN samples used in this work. Altogether, 12 thin film samples grown by two different techniques are studied here. Detailed specifications of the samples along with the TDTR-measured room-temperature thermal conductivities are provided in Table I.

III. RESULTS AND DISCUSSION

The TDTR-measured room-temperature thermal conductivities of the homoepitaxial GaN films as a function of film thickness are presented in Fig. 2. For comparison, we also include the thermal conductivity of other homoepitaxially [6] and heteroepitaxially [15,36] grown GaN films from the literature, and first-principles lattice dynamics (FPLD) predictions of pristine GaN thermal conductivity as a function of thickness (see Supplemental Material for details [35,37–39]). The measurements presented in this figure allow us to isolate the role of size effects and doping on the thermal conductivity of homoepitaxial GaN films.

TABLE I. Specifications and room-temperature thermal conductivities of the GaN thin films used in this work. Details of the uncertainty calculations are provided in the Supplemental Material [35].

Growth technique	Film thickness (μm)	Doping type	Substrate/template	Thermal conductivity (W m^{-1} K^{-1})
MOCVD	0.25	UID	n-doped HVPE	150 ± 50
	0.5		GaN substrate [40]	158 ± 40
	1			176 ± 30
	1.9			196 ± 20
	2.03			203 ± 16
	2.1			195 ± 20
MBE	0.4	UID		168 ± 18
	0.8	UID		167 ± 23
	0.4	10^{18} cm^{-3} Mg-doped	1.8 μm Fe-doped	81 ± 14
	0.8	10^{18} cm^{-3} Mg-doped	GaN template [41]	72 ± 14
	0.4	10^{19} cm^{-3} Mg-doped	on sapphire substrate	59 ± 11
	0.8	10^{19} cm^{-3} Mg-doped		55 ± 14

The silicon, carbon, and oxygen impurity concentrations of our UID GaN films range from 10^{15} to 2×10^{17} cm^{-3}. In addition, the films have a dislocation density on the order of $\sim 10^{8}$ cm^{-2} or less. At room temperature, these concentrations of defects and dislocations are not expected to have a significant effect on GaN thermal conductivity [8,14,42,43]. As a result, the thermal conductivities of the UID GaN films are higher than other heteroepitaxially grown GaN films [36] of equivalent thicknesses reported in the literature. Such heteroepitaxial GaN films can contain high concentrations of point defects and dislocations [15,36,44]. Within uncertainty, the thermal conductivities of our UID GaN films are in agreement with the FPLD predictions of pristine GaN. The higher mean thermal conductivities of the GaN films compared to the FPLD predictions indicate that scattering at the GaN/GaN interface may not be completely diffusive as assumed in the first-principles calculations [45,46].

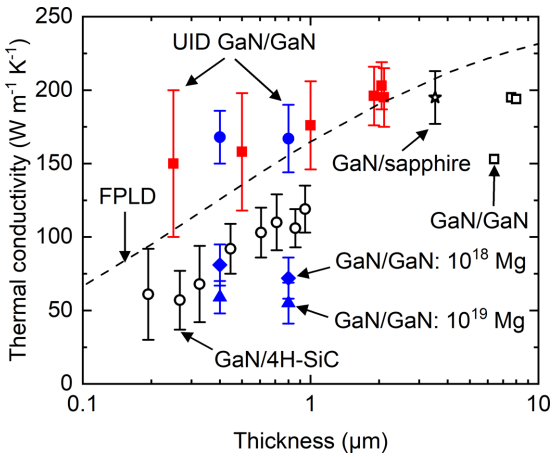

FIG. 2. Room-temperature thermal conductivity as a function of film thickness for MOCVD-grown (red symbols) and MBE-grown (blue symbols) GaN thin films of this study. For comparison, we also include the literature reported thermal conductivities of other homoepitaxially [6] and heteroepitaxially (GaN/sapphire [15] and GaN/4H-SiC [36]) grown GaN films. The dashed line represents the FPLD predictions of defect-free and single-crystalline GaN. Solid and open symbols represent measurements taken in this work and literature values, respectively.

When the MBE-grown GaN films are doped with 10^{18} and 10^{19} cm^{-3} Mg, the thermal conductivity decreases by more than 50%. This is in alignment with the findings of Zou *et al.* [8]. The concentrations of Mg dopants used in this study are not enough to cause a large lattice strain that can lead to significant phonon scattering [47–51]. Therefore, the large thermal conductivity decrease provides evidence that at room temperature, phonon-dopant scattering is dominating the thermal resistance of the homoepitaxial Mg-doped GaN films. Four-point probe measurements reveal that the electrical resistivity of the GaN films decreases from $\sim$0.85 to 0.30 Ω cm as the dopant concentration increases from 10^{18} to 10^{19} cm^{-3}, respectively. However, the corresponding changes in the thermal conductivity for the two dopant concentrations are negligible showing the phonon-dominated nature of thermal transport in GaN thin films.

In addition to TDTR, we have also used the recently developed pump-probe technique SSTR to measure the room-temperature thermal conductivity of several control GaN samples as discussed in the Supplemental Material [35]. Within uncertainty, the TDTR- and SSTR-measured values are in excellent agreement as exhibited in Table S1. Details of our TDTR and SSTR setups, measurement procedures, and analyses are provided in the Supplemental Material [35].

In Fig. 3, we present the TDTR-measured temperature-dependent thermal conductivity of the 1.9 μm MOCVD-grown UID GaN, and 0.8 μm MBE-grown UID and Mg-doped GaN films. For the MBE-grown films, we have limited the measurements down to 200 K, as below this temperature, TDTR measurements become highly sensitive to the Fe-doped GaN template. As the temperature (T) approaches the Debye temperature, the thermal conductivity of a high-purity, bulk, crystalline material can be expected to follow a $1/T^{m}$ ($m = 1$–1.5) trend due to the dominance of phonon-phonon scattering [6,61–63]. As shown in Fig. 3, a $1/T^{1.35}$ relation fits the thermal conductivity of the 1.9 μm UID GaN (Debye temperature $\sim$636 K [64]) film reasonably well from $\sim$200

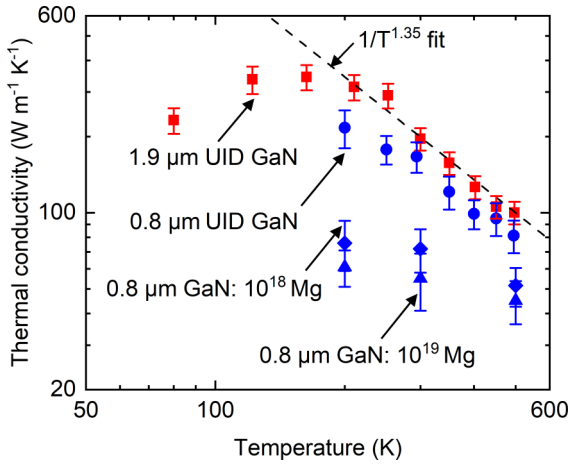

FIG. 3. Temperature-dependent thermal conductivity of the 1.9 μm UID GaN, and 0.8 μm UID and Mg-doped GaN films. The dashed line represents the $A/T^{1.35}$ ($A = 4.4 \times 10^5$) function used to fit the 1.9 μm GaN thermal conductivity from ~200 to 495 K. The red and blue symbols represent MOCVD-grown and MBE-grown samples, respectively.

to 495 K. We attribute the deviation below 200 K to the dominance of phonon-boundary scattering at the GaN/GaN interface and phonon-defect scattering in the film that becomes more prominent at low temperatures [16,54]. Similarly, due to size effects [12,65,66], the thermal conductivity of the 0.8 μm UID GaN film is lower compared to the 1.9 μm film at nearly all temperatures. The thermal conductivities of the Mg-doped GaN films are also significantly reduced because of phonon-dopant scattering and size effects. This figure provides evidence that phonon-boundary scattering can limit the thermal transport in homoepitaxially grown GaN thin films, particularly below 200 K.

Contrary to the MOCVD-grown GaN films, in MBE-grown films, Al is deposited atop the GaN *in situ* under ultrahigh vacuum. We measure the thermal boundary conductance at this interface with TDTR. Our measured data along with other literature reported metal/GaN thermal boundary conductances are presented in Fig. 4(a) as a function of metal elastic modulus. As evident here, the thermal boundary conductance at different metal/GaN interfaces does not exhibit any visible trend with elastic modulus. Donovan *et al.* [56] also noticed a similar phenomena with metal Debye temperatures. These provide evidence that instead of the intrinsic properties of the metallic layers (e.g., elastic modulus, sound speed, and Debye temperature), extrinsic factors such as interface quality and chemistry most likely contributed to prior reports on the thermal boundary conductance across the metal/GaN interfaces [56,67–69]. As the Al deposition on the MBE-grown films is done *in situ* under ultrahigh vacuum, the effects of such extrinsic factors are relatively minimal in our data. Therefore, the thermal boundary conductance at this Al/GaN interface, to the best of our knowledge, is the highest reported to date among metal/GaN interfaces. We have limited our measurements to the MBE-grown films here as the MOCVD-grown films can suffer from the aforementioned extrinsic factors.

In Fig. 4(b), we present the temperature-dependent Al/GaN thermal boundary conductance of the MBE-grown thin films. For comparison, we also include Al/GaN and Al/Ti/GaN thermal boundary conductances from Donovan *et al.* [56], and predictions of the modal nonequilibrium Landauer method for an Al/GaN interface (see Supplemental Material [35,70]). Due to the extrinsic interfacial factors and quality considerations, the Al/GaN and Al/Ti/GaN thermal boundary conductances from Donovan *et al.* [56] are lower than our measured Al/GaN values. In addition, our Al/GaN thermal boundary conductances are in agreement with the predictions of the modal nonequilibrium Landauer method. This modified Landauer approach considers only the elastic phonon scattering process at the Al/GaN interface. Thus, the agreement shown in Fig. 4(b) indicates that the thermal transport at the Al/GaN interface has negligible contributions from inelastic electron or phonon processes [69]. Similar elastic

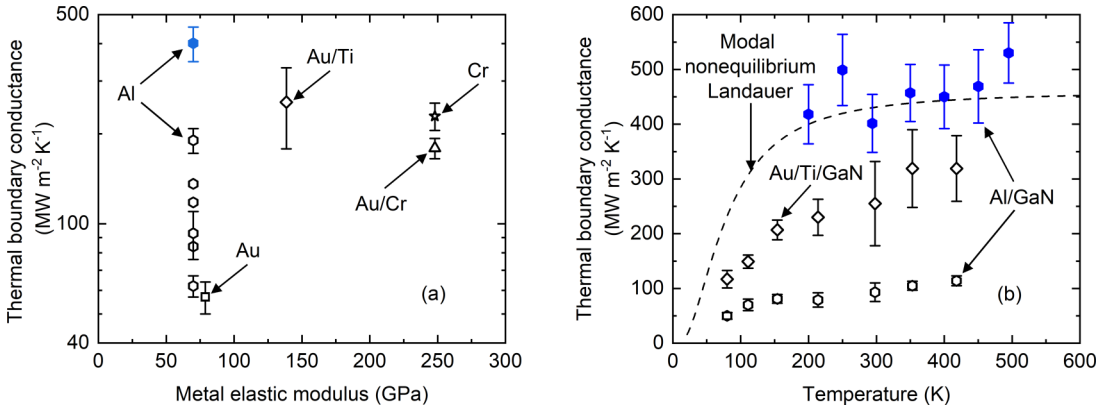

FIG. 4. (a) Room-temperature metal/GaN thermal boundary conductance as a function of elastic modulus for different metals. The solid symbol represents the MBE-grown GaN films measured in this study and open symbols represent different metal/GaN interfaces [52–56] compiled from Donovan *et al.* [56]. For cases where an adhesion layer is present at the interface (Au/Ti and Au/Cr), the elastic modulus [57–60] corresponds to the layer in contact with the GaN. (b) Temperature-dependent Al/GaN thermal boundary conductance for the MBE-grown films. For comparison, we also include the Au/Ti/GaN and Al/GaN thermal boundary conductances from literature [56]. The dashed line represents the thermal boundary conductance predicted by the modal nonequilibrium Landauer method for an Al/GaN interface.

phonon-dominated thermal boundary conductances have also been observed at Al/sapphire, Ru/sapphire, and Co/sapphire interfaces in our previous publication [69]. The fundamental insights provided here into the thermal transport mechanisms at the metal/GaN interfaces are of significant technological importance [56,71,72].

IV. CONCLUSIONS

In summary, we report on the thermal conductivity of a series of homoepitaxially grown GaN films with thicknesses ranging from 0.25 to 2.1 μm. The films are grown by two different techniques: MOCVD and MBE. The homoepitaxial UID GaN films possess lower concentrations of point defects and dislocations, resulting in higher thermal conductivities as compared to other heteroepitaxially grown GaN films of equivalent thicknesses reported in the literature. Doping with Mg results in thermal conductivity reductions by more than 50% revealing that the dominant source of phonon scattering in homoepitaxially grown GaN films is the dopants. Scattering with the defects and GaN/GaN interface also starts to play an important role in limiting the thermal conductivity of the UID GaN films below 200 K. Furthermore, due to *in situ* deposition of Al in ultrahigh vacuum, the Al/GaN thermal boundary conductance of the MBE-grown films, to the best of our knowledge, is the highest reported to date among metal/GaN interfaces. The interfacial thermal transport at this Al/GaN interface is dominated by elastic phonon scattering. The findings presented in this paper are of crucial importance in isolating the role of size effects and phonon-dopant scattering on limiting the thermal conductivity of submicrometer and micrometer thick GaN thin films.

ACKNOWLEDGMENTS

We appreciate support from the Office of Naval Research under a MURI program, Grant No. N00014-18-1-2429. J.K.H. acknowledges that the work at the Naval Research Laboratory (NRL) is financially supported by the Office of Naval Research.

[1] F. Mu, Z. Cheng, J. Shi, S. Shin, B. Xu, J. Shiomi, S. Graham, and T. Suga, ACS Appl. Mater. Interfaces **11**, 33428 (2019).
[2] Z. Cheng, F. Mu, L. Yates, T. Suga, and S. Graham, ACS Appl. Mater. Interfaces **12**, 8376 (2020).
[3] D. Kotchetkov, J. Zou, A. Balandin, D. Florescu, and F. H. Pollak, Appl. Phys. Lett. **79**, 4316 (2001).
[4] L. Lindsay, D. A. Broido, and T. L. Reinecke, Phys. Rev. Lett. **109**, 095901 (2012).
[5] A. L. Moore and L. Shi, Mater. Today **17**, 163 (2014).
[6] Q. Zheng, C. Li, A. Rai, J. H. Leach, D. A. Broido, and D. G. Cahill, Phys. Rev. Materials **3**, 014601 (2019).
[7] C. Mion, J. Muth, E. A. Preble, and D. Hanser, Superlattices Microstruct. **40**, 338 (2006).
[8] J. Zou, D. Kotchetkov, A. Balandin, D. Florescu, and F. H. Pollak, J. Appl. Phys. **92**, 2534 (2002).
[9] T. Wang, J. Carrete, N. Mingo, and G. K. Madsen, ACS Appl. Mater. Interfaces **11**, 8175 (2019).
[10] Y. R. Koh, H. Lu, A. C. Gossard, and A. Shakouri, Nanotechnology **32**, 035702 (2020).
[11] M. Kamatagi, R. Vaidya, N. Sankeshwar, and B. Mulimani, Int. J. Heat Mass Transfer **52**, 2885 (2009).
[12] T. E. Beechem, A. E. McDonald, E. J. Fuller, A. A. Talin, C. M. Rost, J.-P. Maria, J. T. Gaskins, P. E. Hopkins, and A. A. Allerman, J. Appl. Phys. **120**, 095104 (2016).
[13] M. Souissi, T. Ghrib, A. Al-Otaibi, I. Al-Nuaim, and M. Bouzidi, Thermochim. Acta **682**, 178428 (2019).
[14] B. Sun, G. Haunschild, C. Polanco, L. Lindsay, G. Koblmüller, Y. K. Koh *et al.*, Nat. Mater. **18**, 136 (2019).
[15] H. Li, R. Hanus, C. A. Polanco, A. Zeidler, G. Koblmüller, Y. K. Koh, and L. Lindsay, Phys. Rev. B **102**, 014313 (2020).
[16] M. S. B. Hoque, Y. R. Koh, J. L. Braun, A. Mamun, Z. Liu, K. Huynh, M. E. Liao, K. Hussain, Z. Cheng, E. R. Hoglund *et al.*, ACS Nano **15**, 9588 (2021).
[17] D. G. Cahill, Rev. Sci. Instrum. **75**, 5119 (2004).
[18] A. J. Schmidt, X. Chen, and G. Chen, Rev. Sci. Instrum. **79**, 114902 (2008).
[19] P. E. Hopkins, J. R. Serrano, L. M. Phinney, S. P. Kearney, T. W. Grasser, and C. T. Harris, J. Heat Transfer **132**, 081302 (2010).
[20] J. P. Feser, J. Liu, and D. G. Cahill, Rev. Sci. Instrum. **85**, 104903 (2014).
[21] F. Krahl, A. Giri, M. S. B. Hoque, L. Sederholm, P. E. Hopkins, and M. Karppinen, J. Phys. Chem. C **124**, 24731 (2020).
[22] J. L. Braun, D. H. Olson, J. T. Gaskins, and P. E. Hopkins, Rev. Sci. Instrum. **90**, 024905 (2019).
[23] M. S. B. Hoque, Y. R. Koh, K. Aryana, E. R. Hoglund, J. L. Braun, D. H. Olson, J. T. Gaskins, H. Ahmad, M. M. M. Elahi, J. K. Hite, Z. C. Leseman, W. A. Doolittle, and P. E. Hopkins, Rev. Sci. Instrum. **92**, 064906 (2021).
[24] E. Jang, P. Banerjee, J. Huang, R. Holley, J. T. Gaskins, M. S. B. Hoque, P. E. Hopkins, and D. Madan, Electronics **9**, 532 (2020).
[25] J. Hite, T. Anderson, L. Luna, J. Gallagher, M. Mastro, J. Freitas, and C. Eddy, Jr., J. Cryst. Growth **498**, 352 (2018).
[26] E. A. Scott, K. Hattar, J. L. Braun, C. M. Rost, J. T. Gaskins, T. Bai, Y. Wang, C. Ganski, M. Goorsky, and P. E. Hopkins, Carbon **157**, 97 (2020).
[27] Y. Wang, J. Y. Park, Y. K. Koh, and D. G. Cahill, J. Appl. Phys. **108**, 043507 (2010).
[28] R. Wilson, B. A. Apgar, L. W. Martin, and D. G. Cahill, Opt. Express **20**, 28829 (2012).
[29] L. Wang, R. Cheaito, J. Braun, A. Giri, and P. Hopkins, Rev. Sci. Instrum. **87**, 094902 (2016).
[30] C. M. Rost, J. Braun, K. Ferri, L. Backman, A. Giri, E. J. Opila, J.-P. Maria, and P. E. Hopkins, Appl. Phys. Lett. **111**, 151902 (2017).
[31] R. S. Waremra and P. Betaubun, E3S Web Conf. **73**, 13019 (2018).
[32] B. Heying, I. Smorchkova, C. Poblenz, C. Elsass, P. Fini, S. Den Baars, U. Mishra, and J. Speck, Appl. Phys. Lett. **77**, 2885 (2000).
[33] E. Glaser, M. Murthy, J. Freitas, Jr., D. Storm, L. Zhou, and D. Smith, Phys. B: Condens. Matter **401**, 327 (2007).

[34] Y.-Z. Wu, B. Liu, Z.-H. Li, T. Tao, Z.-L. Xie, X.-Q. Xiu, P. Chen, D.-J. Chen, H. Lu, Y. Shi *et al.*, J. Cryst. Growth **506**, 30 (2019).

[35] See Supplemental Material at http://link.aps.org/supplemental/10.1103/PhysRevMaterials.5.104604 for additional details of the cleaning process of MBE-grown samples, and first-principles lattice dynamics calculations.

[36] E. Ziade, J. Yang, G. Brummer, D. Nothern, T. Moustakas, and A. J. Schmidt, Appl. Phys. Lett. **110**, 031903 (2017).

[37] S. Baroni, S. De Gironcoli, A. Dal Corso, and P. Giannozzi, Rev. Mod. Phys. **73**, 515 (2001).

[38] P. Giannozzi, S. Baroni, N. Bonini, M. Calandra, R. Car, C. Cavazzoni, D. Ceresoli, G. L. Chiarotti, M. Cococcioni, I. Dabo *et al.*, J. Phys.: Condens. Matter **21**, 395502 (2009).

[39] W. Li, J. Carrete, N. A. Katcho, and N. Mingo, Comput. Phys. Commun. **185**, 1747 (2014).

[40] J. Gallagher, T. Anderson, L. Luna, A. Koehler, J. Hite, N. Mahadik, K. Hobart, and F. Kub, J. Cryst. Growth **506**, 178 (2019).

[41] H. Ahmad, T. J. Anderson, J. C. Gallagher, E. A. Clinton, Z. Engel, C. M. Matthews, and W. Alan Doolittle, J. Appl. Phys. **127**, 215703 (2020).

[42] G. A. Slack, L. J. Schowalter, D. Morelli, and J. A. Freitas, Jr., J. Cryst. Growth **246**, 287 (2002).

[43] R. B. Simon, J. Anaya, and M. Kuball, Appl. Phys. Lett. **105**, 202105 (2014).

[44] K. Park and C. Bayram, J. Appl. Phys. **126**, 185103 (2019).

[45] T. Zeng and G. Chen, J. Heat Transfer **123**, 340 (2001).

[46] Y. R. Koh, Z. Cheng, A. Mamun, M. S. Bin Hoque, Z. Liu, T. Bai, K. Hussain, M. E. Liao, R. Li, J. T. Gaskins *et al.*, ACS Appl. Mater. Interfaces **12**, 29443 (2020).

[47] P. Prystawko, M. Leszczynski, B. Beaumont, P. Gibart, E. Frayssinet, W. Knap, P. Wisniewski, M. Bockowski, T. Suski, and S. Porowski, Phys Status Solidi B **210**, 437 (1998).

[48] M. Leszczynski, P. Prystawko, T. Suski, B. Lucznik, J. Domagala, J. Bak-Misiuk, A. Stonert, A. Turos, R. Langer, and A. Barski, J. Alloys Compd. **286**, 271 (1999).

[49] C. G. Van de Walle, Phys. Rev. B **68**, 165209 (2003).

[50] A. Jeżowski, B. Danilchenko, M. Boćkowski, I. Grzegory, S. Krukowski, T. Suski, and T. Paszkiewicz, Solid State Commun. **128**, 69 (2003).

[51] J. Kim, O. Seo, C. Song, S. Hiroi, Y. Chen, Y. Irokawa, T. Nabatame, Y. Koide, and O. Sakata, CrystEngComm **21**, 2281 (2019).

[52] R. J. Stevens, L. V. Zhigilei, and P. M. Norris, Int. J. Heat Mass Transfer **50**, 3977 (2007).

[53] X. W. Zhou, R. E. Jones, C. J. Kimmer, J. C. Duda, and P. E. Hopkins, Phys. Rev. B **87**, 094303 (2013).

[54] J. P. Freedman, J. H. Leach, E. A. Preble, Z. Sitar, R. F. Davis, and J. A. Malen, Sci. Rep. **3**, 2963 (2013).

[55] J. Cho, Y. Li, W. E. Hoke, D. H. Altman, M. Asheghi, and K. E. Goodson, Phys. Rev. B **89**, 115301 (2014).

[56] B. F. Donovan, C. J. Szwejkowski, J. C. Duda, R. Cheaito, J. T. Gaskins, C.-Y. Peter Yang, C. Constantin, R. E. Jones, and P. E. Hopkins, Appl. Phys. Lett. **105**, 203502 (2014).

[57] B. Halg, IEEE Trans. Electron Devices **37**, 2230 (1990).

[58] M. C. Salvadori, I. G. Brown, A. R. Vaz, L. L. Melo, and M. Cattani, Phys. Rev. B **67**, 153404 (2003).

[59] S. G. Nilsson, X. Borrise, and L. Montelius, Appl. Phys. Lett. **85**, 3555 (2004).

[60] W.-d. Zhang, Y. Liu, H. Wu, M. Song, T.-y. Zhang, X.-d. Lan, and T.-h. Yao, Mater. Charact. **106**, 302 (2015).

[61] G. A. Slack, R. A. Tanzilli, R. Pohl, and J. Vandersande, J. Phys. Chem. Solids **48**, 641 (1987).

[62] G. Chen, *Nanoscale Energy Transport and Conversion: A Parallel Treatment of Electrons, Molecules, Phonons, and Photons* (Oxford University Press, Oxford, UK, 2005).

[63] Z. Guo, A. Verma, X. Wu, F. Sun, A. Hickman, T. Masui, A. Kuramata, M. Higashiwaki, D. Jena, and T. Luo, Appl. Phys. Lett. **106**, 111909 (2015).

[64] K. Adachi, H. Ogi, A. Nagakubo, N. Nakamura, M. Hirao, M. Imade, M. Yoshimura, and Y. Mori, J. Appl. Phys. **119**, 245111 (2016).

[65] R. Cheaito, J. C. Duda, T. E. Beechem, K. Hattar, J. F. Ihlefeld, D. L. Medlin, M. A. Rodriguez, M. J. Campion, E. S. Piekos, and P. E. Hopkins, Phys. Rev. Lett. **109**, 195901 (2012).

[66] J. L. Braun, C. H. Baker, A. Giri, M. Elahi, K. Artyushkova, T. E. Beechem, P. M. Norris, Z. C. Leseman, J. T. Gaskins, and P. E. Hopkins, Phys. Rev. B **93**, 140201(R) (2016).

[67] P. E. Hopkins, L. M. Phinney, J. R. Serrano, and T. E. Beechem, Phys. Rev. B **82**, 085307 (2010).

[68] C. S. Gorham, K. Hattar, R. Cheaito, J. C. Duda, J. T. Gaskins, T. E. Beechem, J. F. Ihlefeld, L. B. Biedermann, E. S. Piekos, D. L. Medlin, and P. E. Hopkins, Phys. Rev. B **90**, 024301 (2014).

[69] Y. R. Koh, J. Shi, B. Wang, R. Hu, H. Ahmad, S. Kerdsongpanya, E. Milosevic, W. A. Doolittle, D. Gall, Z. Tian, S. Graham, and P. E. Hopkins, Phys. Rev. B **102**, 205304 (2020).

[70] J. Shi, X. Yang, T. S. Fisher, and X. Ruan, arXiv:1812.07910.

[71] R. M. Costescu, M. A. Wall, and D. G. Cahill, Phys. Rev. B **67**, 054302 (2003).

[72] Y. K. Koh and D. G. Cahill, Phys. Rev. B **76**, 075207 (2007).